

# Aptamer-Mediated Nanoparticle-Based Protein Labeling Platform for Intracellular Imaging and Tracking Endocytosis Dynamics

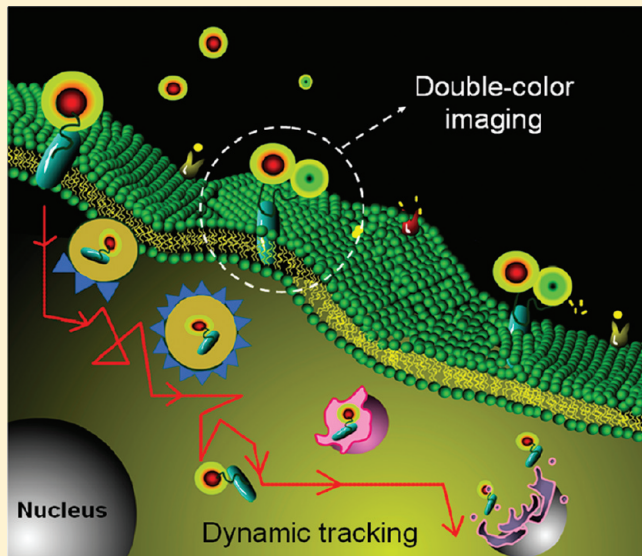
Li Qiang Chen,<sup>†,||</sup> Sai Jin Xiao,<sup>†</sup> Ping Ping Hu,<sup>†,‡</sup> Li Peng,<sup>†,‡</sup> Jun Ma,<sup>‡</sup> Ling Fei Luo,<sup>‡</sup> Yuan Fang Li,<sup>†</sup> and Cheng Zhi Huang<sup>\*,†,§</sup>

<sup>†</sup>Education Ministry Key Laboratory on Luminescence and Real-Time Analysis, College of Pharmaceutical Sciences, <sup>‡</sup>College of Life Sciences, and <sup>§</sup>College of Chemistry and Chemical Engineering, Southwest University, Chongqing 400054, People's Republic of China

<sup>||</sup>Asian International Rivers Center, Yunnan Key Laboratory of International Rivers and Transboundary Eco-security, Yunnan University, Kunming 650091, People's Republic of China

## Supporting Information

**ABSTRACT:** Although nanoparticles have been widely used as optical contrasts for cell imaging, the complicated prefunctionalized steps and low labeling efficiency of nanoprobes greatly inhibit their applications in cellular protein imaging. In this study, we developed a novel and general strategy that employs an aptamer not only as a recognizer for protein recognition but also as a linker for nanoreporter targeting to specifically label membrane proteins of interest and track their endocytic pathway. With this strategy, three kinds of nanoparticles, including gold nanoparticles, silver nanoparticles, and quantum dots (QDs), have been successfully targeted to the membrane proteins of interest, such as nucleolin or prion protein ( $\text{PrP}^{\text{C}}$ ). The following investigations on the subcellular distribution with fluorescent immunocolocalization assay indicated that  $\text{PrP}^{\text{C}}$ -aptamer-QD complexes most likely internalized into cytoplasm through a classical clathrin-dependent/receptor-mediated pathway. Further single-particle tracking and trajectory analysis demonstrated that  $\text{PrP}^{\text{C}}$ -aptamer-QD complexes exhibited a complex dynamic process, which involved three types of movements, including membrane diffusion, vesicle transportation, and confined diffusion, and all types of these movements were associated with distinct phases of  $\text{PrP}^{\text{C}}$  endocytosis. Compared with traditional multilayer methods, our proposed aptamer-mediated strategy is simple in procedure, avoiding any complicated probe premodification and purification. In particular, the new double-color labeling strategy is unique and significant due to its superior advantages of targeting two signal reporters simultaneously in a single protein using only one aptamer. What is more important, we have constructed a general and versatile aptamer-mediated protein labeling nanoplateform that has shown great promise for future biomedical labeling and intracellular protein dynamic analysis.



Visualization of disease-related protein dynamic processes within living cells is of fundamental importance for deciphering the pathological processes and may provide new insight for scientists into the molecular details of intracellular transport of disease-related proteins in living cells.<sup>1,2</sup> Although traditional fluorescence labeling and imaging techniques have been widely adopted for this purpose, the weak fluorescent emission and fast photobleaching of single fluorescent dye molecules makes the imaging and tracking of single biological molecules in living cells a challenge. Novel fluorescent nanoprobes possess excellent optical properties such as exceptional brightness, diameter-dependent multicolors, and nonphotobleaching, thus providing us an opportunity to use

these nanoprobes as novel optical contrasts for real-time protein imaging and dynamic tracking.<sup>3</sup>

However, current nanoprobes are often targeted to the protein of interest with an antibody-based multilayer strategy that requires the nanoprobes to be elaborately prefunctionalized with many heavy and complicated modification steps, such as covalent bonding with streptavidin and linkage with biotinylated primary antibody followed by secondary antibody attachment (Scheme 1a). These multilayer modifications may

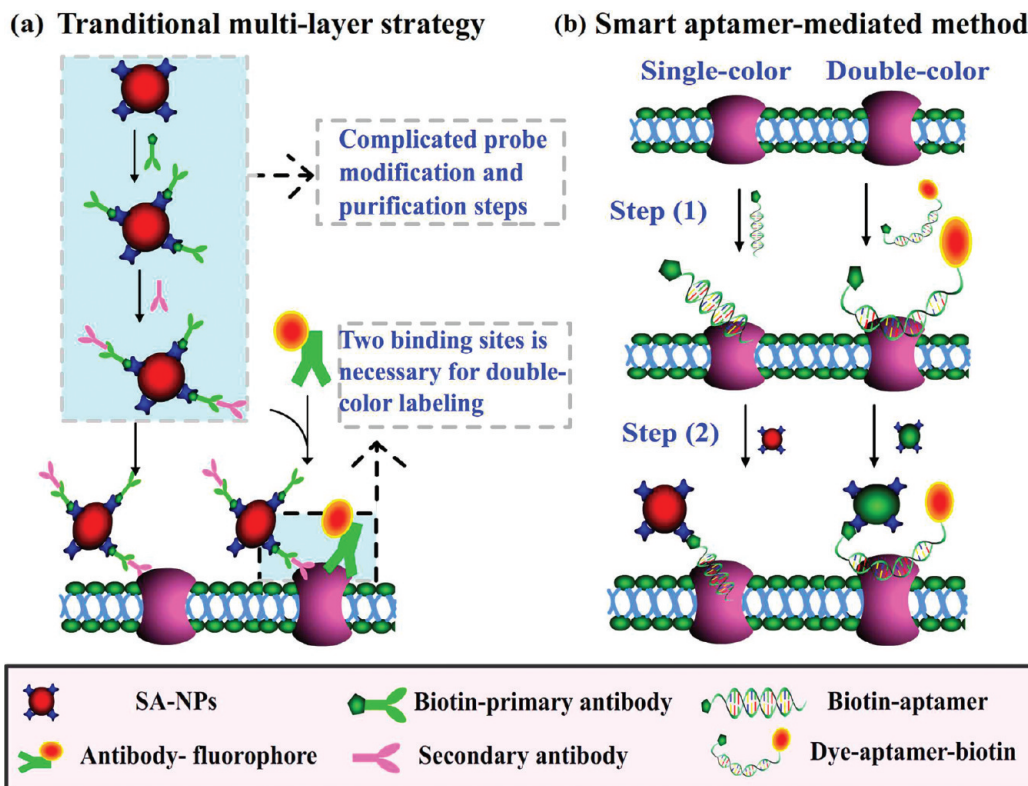
Received: October 24, 2011

Accepted: February 27, 2012

Published: February 27, 2012



**Scheme 1.** Principle of the Traditional Multi-layer-Based Method (a) and Our Smart Aptamer-Mediated Strategy (b) for Cell Surface Protein Labeling<sup>a</sup>



<sup>a</sup>The traditional labeling method for targeting nanoparticles to cell surface proteins by using complicated multilayer modification of nanoparticles with streptavidin, biotin-modified primary antibody, and secondary antibody attachment obviously increases the size and decreases the stability of nanoprobes. Our present aptamer-mediated strategy for single-color or double-color labeling of a cell surface protein follows two steps: step 1, the cell surface protein was first targeted with biotin-aptamer added; step 2, biotinylated protein was recognized by SA-NPs to achieve the label.

greatly reduce the stability and increase the steric hindrance of the nanoprobes with the result of restricting access to certain regions of the cell surface and impairing endocytosis.<sup>4,5</sup> In addition, if a double-color label is required, there must be two binding sides in one target protein, which usually is not desired.

Aptamer-conjugated nanoparticles as sensing systems that combine the specific molecular recognition of aptamers with the strong signal transduction capacity of nanoparticles offer an alternative approach for cell labeling and imaging.<sup>6</sup> Compared to antibodies, aptamers have similarly high affinity and selectivity for proteins, but their superior properties of small size and easy modification can effectively reduce the steric hindrance and simplify the modification steps of nanoprobes, thereby facilitating the procedure and improving the target recognition performance.<sup>7,8</sup> Consequently, aptamer-conjugated nanoparticles as probes have been widely used for disease-associated isoform discrimination,<sup>9</sup> virus labeling,<sup>10</sup> multifunctional cell imaging,<sup>11–13</sup> and cancer cell targeting and therapy.<sup>14,15</sup> Although aptamer–nanoparticle-conjugate-based methods have already succeeded in solving some problems in nanoprobe modification, further separation, purification, and quantification of products are troublesome.<sup>16</sup>

Apart from aptamer–nanoparticle-conjugate-based methods, another promising approach for nanoprobe targeting is the small-molecule-based site-specific protein labeling method which was first proposed by Ting's group<sup>4,17</sup> and then successfully applied in various membrane labeling<sup>18,19</sup> and virus tracking<sup>20</sup> techniques. Unfortunately, all of these small

molecular ligands, such as biotin ligase or cutinase,<sup>4,19</sup> still need to be prefused to the target protein with complicated genetic fusion techniques and then expressed, extracted, and purified from bacteria, and these processes have a high labor cost and are time-consuming.

In this study, we developed a simple strategy that needs neither multilayer modifications nor complicated genetic fusion techniques to achieve both site-specific protein labeling and cellular dynamic tracking of target proteins. The key factor of our strategy is to employ an aptamer not only as a recognizer for protein recognition but also as a linker for targeting nanoreporters to proteins of interest. In our approach, a cell membrane protein is previously labeled by adding a biotin-modified aptamer (Bio-Apt) which can specifically recognize the protein of interest, and then the biotin group serves as a handle for targeting streptavidin-conjugated nanoparticles (SA-NPs) (Scheme 1b). Particularly, if dual-color labeling is desired, as shown in Scheme 1b, the only thing that needs to be done is to replace the Bio-Apt with a dual-modified aptamer; namely, both the 3'- and 5'-termini of the aptamer are conjugated with functional groups. This novel double-color labeling method is unique and attractive since it can target two signal reporters synchronously in one protein using a single aptamer. Owing to the avoidance of multiple modification and purification steps of the nanoprobe, our proposed aptamer-mediated method offers a general and versatile nanoplatform for potential labeling and tracking of various proteins in living cells.

## ■ EXPERIMENTAL SECTION

**Reagents.** The biotin-labeled probe or biotin/6-carboxy-X-rhodamine (ROX)-double-labeled probe, based on the 17-nt DNA aptamer of PrP<sup>C</sup> (prion protein), was synthesized by Shenggong Bio Inc. (Shanghai, China). The aptamer sequences, obtained from the literature,<sup>21,22</sup> are as follows: Bio-Apt1, 5'-biotin-(C<sub>6</sub>)-TTG GTG GTG GTG GTT GTG GTG GTG GTG G-3'; Bio-Apt2, 5'-biotin-(C<sub>6</sub>)-CTT ACG GTG GGG CAA TT-3'; Bio-Apt2-ROX, 5'-biotin-(C<sub>6</sub>)-CTT ACG GTG GGG CAA TT-ROX-3'. The control DNA sequence of PolyT<sub>17</sub> is 5'-biotin-(C<sub>6</sub>)-TTT TTT TTT TTT TTT TT-3'. Streptavidin–quantum dot (QD) conjugates were purchased from Jiayuan Quantum Dot Co. Ltd. (Wuhan, China). All cellular organelle specific markers and labeling kits, including Golgi markers of 6-((N-(7-nitrobenz-2-oxa-1,3-diazol-4-yl)amino)hexanoyl)sphingosine (NBD; CN N-1154), BODIPY FL histamine (CN B-22461), SelectFX Alexa Fluor 488 Endoplasmic Reticulum Labeling Kit (CN S-34200), Alexa Fluor 488–transferrin conjugates (CN T-13342), and streptavidin–FITC conjugates, were purchased from Molecular Probes, Inc. (Eugene, OR) and used as received. Rabbit anticalthrin heavy chain antibody and Alexa Fluor 488-conjugated goat polyclonal rabbit IgG (H+L) were obtained from Abcam, Inc. (Hong Kong). Membrane dye 3,3'-dioctadecyloxacarbocyanine perchlorate (DIO) and nucleolus dye Hoechst 33258 were both obtained from Sigma, Inc. (Shanghai, China). Other commercial reagents were analytical reagent grade and were used without further purification. All water used was ultrapurified with an LD-50G-E Ultra-Pure Water System (Lidi Modern Waters Equipments Co., Chongqing, China).

**Preparation of Streptavidin–Nanoparticle Conjugates.** Silver nanoparticles (AgNPs) and gold nanoparticles (AuNPs) were prepared according to the modified Lee–Meisel method.<sup>23</sup> The size of the nanoparticles as-prepared was measured with a Hitachi S-4800 scanning electron microscope (Tokyo, Japan), and the concentration was calculated according to the extinction of the colloidal solution.<sup>24</sup> These nanoparticles were functionalized with streptavidin according to our reported methods that modified gold nanoparticles with minor modifications.<sup>11,25</sup> The UV/vis spectrum of the nanoparticle solution was measured with a UV-3600 UV/vis/NIR spectrophotometer (Shimadzu, Japan).

**Cell Culture and Treatment.** HeLa cells and SK-N-SH cells were cultured in flasks in minimum Eagle's essential medium (MEM) supplemented with 10% fetal bovine serum (FBS; Gibco) and 100 IU/mL penicillin–streptomycin at 37 °C under 5% humidified CO<sub>2</sub>. Upon reaching confluence, the cells were trypsinized and replanted at a density of 1 × 10<sup>6</sup> cells/mL onto poly-L-lysine-coated coverslips and grown at 37 °C under 5% humidified CO<sub>2</sub> for 48 h. The cell density was determined using a hemocytometer, and this was performed prior to any experiments. For QD labeling, the cells were rinsed gently with prewarmed phosphate-buffered saline (PBS) and incubated with 200 nM Bio–Apt (or Bio–Apt–ROX for double-color labeling) in MEM for 15 min at 37 °C. After that, the cells were gently rinsed twice with PBS to remove unbound Bio–Apt, followed by replacement with a mixture of cell media and 1 nM SA–QDs. After incubation for a certain time (30–90 min), the cells were rinsed three times with prewarmed PBS to remove unbound SA–QDs and awaited further treatments such as dyeing or fixation.

**Dark-Field Cell Imaging.** In a typical experiment, a 1 mL suspension of HeLa cells (about 10<sup>5</sup> cells/mL) was plated onto a coverslip, and the cells were grown for 1 days. Then the cells were treated with 200 nM Bio–Apt conjugates (or the same concentration of Bio–PolyT as a control) for 15 min, followed by replacement with cell media containing 2.0 pM SA–NPs for 30 min, rinsed with PBS buffer three times, fixed with 4% paraformaldehyde, and sealed with a small amount of glycerol. Dark-field imaging of the cells was acquired with an Olympus BX-51 microscope (Tokyo, Japan), which was equipped with a highly numerical dark-field condenser (U-DCW). Colorful dark-field light scattering photographs of the cells were captured with an Olympus DP72 digital camera (Tokyo, Japan).

**Immunocolocalization with Organelles.** Differentiated SK-N-SH cells were treated with Bio–Apt and SA–QDs, after removal of unbound QDs by washing. The cells were then fixed with 4% paraformaldehyde for 30 min. For nucleolus dyeing, Hoechst 33258 (Sigma) was dissolved in 1 mL of water to give a stock solution of 1.2 mg/mL (2 mM). The cells were stained with PBS mixed with Hoechst 33258 for 10 min and then washed with PBS three times. For membrane dyeing, DIO (Sigma) was dissolved at a final concentration of 1 mg/mL in ethanol and incubated with the cells for 30 min. After being washed with PBS, the cells were blocked out with glycerin and mounted for final imaging.

For transferrin colocalization, the cells were first treated with 200 nM Bio–Apt conjugates for 15 min, followed by replacement with cell media containing 1 nM SA–QDs and 500 nM Alexa Fluor 488–transferrin conjugates for another 30 min. For clathrin staining, SK-N-SH cells were fixed with paraformaldehyde, permeabilized with 0.5% TX-100, and blocked with 1% BSA for 30 min at 22 °C, and then the samples were incubated with rabbit anticalthrin heavy chain antibody at 1/500 dilution (in 1% BSA/PBS) for 1 h at 22 °C. An Alexa Fluor 488-conjugated goat polyclonal rabbit IgG (H+L) was used as a secondary antibody at 1/400 dilution. After washing and nucleolus dyeing, the cells were fixed and mounted for microscope observation. Fluorescent images were acquired on a Zeiss LSM 510 META laser scanning confocal microscope equipped with argon, red He/Ne, and green HeNe lasers. Images were acquired using a 40×/0.95 air objective or a Plan-apochromat 63×/1.4 oil immersion objective. For z axis scanning, micrographs were taken per 0.8 μm while the focal plane was moved in incremental steps from the dish bottom to the top of the cells. Images were analyzed with the use of Zeiss LSM 510 software, version 3.2 SP2. ROX was excited with the 545 nm line of the green HeNe laser, and emission was detected using a 620 nm long-pass filter. The Hoechst 33258 dye was excited with the 405 nm laser line and detected with a 460 nm band-pass filter. The DIO dye was excited at 488 nm and detected at 500–520 nm. QD545 was excited at 340–390 nm (the dichroic mirror was DMS15 nm) and detected with a barrier filter BA518–552 nm. QD605 was excited at 340–390 nm (the dichroic mirror was DM565 nm) and detected with a barrier filter BA595–615 nm.

**Single-Particle Tracking and Trajectory Analysis.** SK-N-SH cells were plated in 35 mm glass bottom culture dishes (MatTek Corp) and grown to 80% confluence for 24 h at 37 °C. After brief incubation with Bio–Apt and then SA–QDs605, followed by rinsing, the cells were incubated on the microscope stage at 37 °C with 5% CO<sub>2</sub>, and image acquisition occurred with a disk scanning unit (DSU) confocal scanning system that

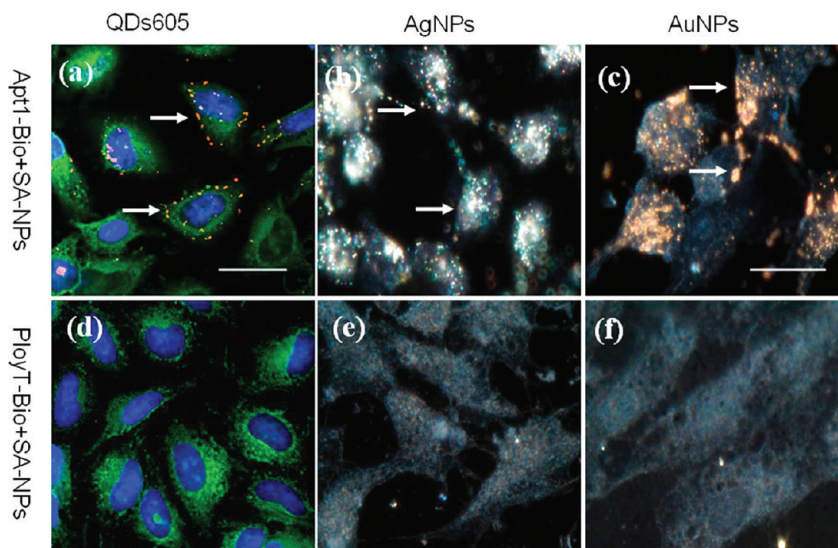


**Figure 1.** Laser confocal fluorescent images and dark-field light scattering images of nucleolin on the surface of HeLa cells: (a) streptavidin-conjugated quantum dots (SA-QDs605); (b) streptavidin-conjugated silver nanoparticles (SA-AgNPs); (c) streptavidin-conjugated gold nanoparticles (SA-AuNPs). HeLa cells showed intense emission (a–c) in the labeling reactions with Bio-Apt1 added, but the signal was abolished (d–f) by replacing Bio-PolyT with Bio-Apt1. The nanoprobes exhibited red (QDs605), white, blue, or green (AgNPs), and gold yellow (AuNPs) color in cell bodies, respectively. Plasmatic membrane dye (DIO) and nucleolus dye (Hoechst 33258) are shown in green color and blue color, respectively. The bar is 30  $\mu$ m for fluorescent images and 20  $\mu$ m for dark-field images.

allows simultaneous detection of QDs and Host33258 fluorescence. The focal plane was fixed on the nucleus plane with a zero drift composition (ZDC). Differential interference contrast (DIC) image acquisition was used for visualization of the complete cells to determine the localization of the QDs in the cell body. Live cell time lapse images were acquired using a DSU confocal microscopy setup consisting of a live cell system and an Olympus IX-81 inverted microscope with an Olympus IX2-DSU confocal scanning system and a Rolera-MGi EM-CCD. Image acquisition (one frame ( $512 \times 512$  pixels) per minute) was taken using In Vivo 3.2/3D Analyzer Suite 6.2 software (MedicaCybernetics, Inc.). QD605 was excited at 340–390 nm (the dichroic mirror was DM565 nm) and detected with a barrier filter BA595–615 nm. The Hoechst 33258 dye was excited with the 405 nm laser line and detected with a 460 nm band-pass filter. For QD imaging, the exposure time was 200 ms and the charge-coupled device (CCD) gain value was 3000. For imaging of the nucleolus, the exposure time was 200 ms and the CCD gain value was decreased to 200.

To determine the average number of PrP<sup>C</sup>-Apt-QD605 complexes per cell from static images, particle counts were obtained from fluorescence images using a dynamic segmentation filter (Image-Pro Plus software (MedicaCybernetics, Inc.)). Dynamic analysis was conducted with the Autotrack function of the Image-Pro Plus software. To monitor and analyze the kinetics of PrP<sup>C</sup>-Apt-QD605 complexes inside the cells, we measured a set group of dynamic characteristics, including velocity, distance, accumulation distance (Acc. Dist.), and the distance from the original starting point (Or. Dist.), and the maximum, minimum, mean, and standard deviation of these characteristics have been recorded. All individual trajectories were visually inspected, and only trajectories were further analyzed in which it was clear that the position of the same PrP<sup>C</sup>-Apt-QD605 conjugate was extracted over the entire duration of the observation.

## RESULTS AND DISCUSSION

**Specificity of the Labeling Strategy.** The principle of our proposal of the aptamer-mediated strategy for single- or double-color labeling of cell surface proteins with nanoparticles is presented in Scheme 1b. To demonstrate the feasibility of our strategy, nucleolin, a biomarker located in the plasma membrane of cancer cells,<sup>26</sup> was selected as the proof-of-concept target. Accordingly, a biotin-modified 28-mer DNA aptamer (Bio-Apt1) that can specifically bind to nucleolin was chosen as the smart recognizer.<sup>21</sup>

After incubation of Bio-Apt1 with HeLa cells (human cervical cancer) for 15 min followed by the addition of SA-QDs605, as shown in Figure 1a, HeLa cells exhibited intense QD605 fluorescence (red dots) in cell bodies, suggesting that cell surface nucleolins were labeled by SA-QD605 conjugates. To test the specificity of such labeling, two control experiments were performed. One control was made by incubating the SA-QDs605 with cells in the absence of Bio-Apt1, and the other was made with nonbiotin-modified aptamers or with a random biotin-modified sequence (Bio-PolyT<sub>17</sub>), followed by addition of SA-QDs605. In both cases, cells displayed minimal red fluorescence from QDs605 in the confocal microscope (Figure 1d and Figure S1 in the Supporting Information), indicating that QDs605 were not attached to cells in the absence of the Bio-Apt1.

These results confirmed that aptamer acts as a recognizer for recognizing protein while biotin acts as a linker for targeting QDs605 to proteins during the labeling processes. Indeed, as we expected, the Bio-Apt1-nucleolin cocktail was formed at first through the specific recognition of Apt1 to nucleolin in the labeling reactions, which allows the biotinylation of nucleolin located on the surface of HeLa cells, and then the surface biotinylation was detected with SA-QDs605. In addition, when SA-QDs605 were replaced with SA-FITC conjugates, the green fluorescent signal of FITC was detectable in the presence of Bio-Apt1, but disappeared in the presence of Bio-PolyT<sub>17</sub> (Figure S2 in the Supporting Information). This result further

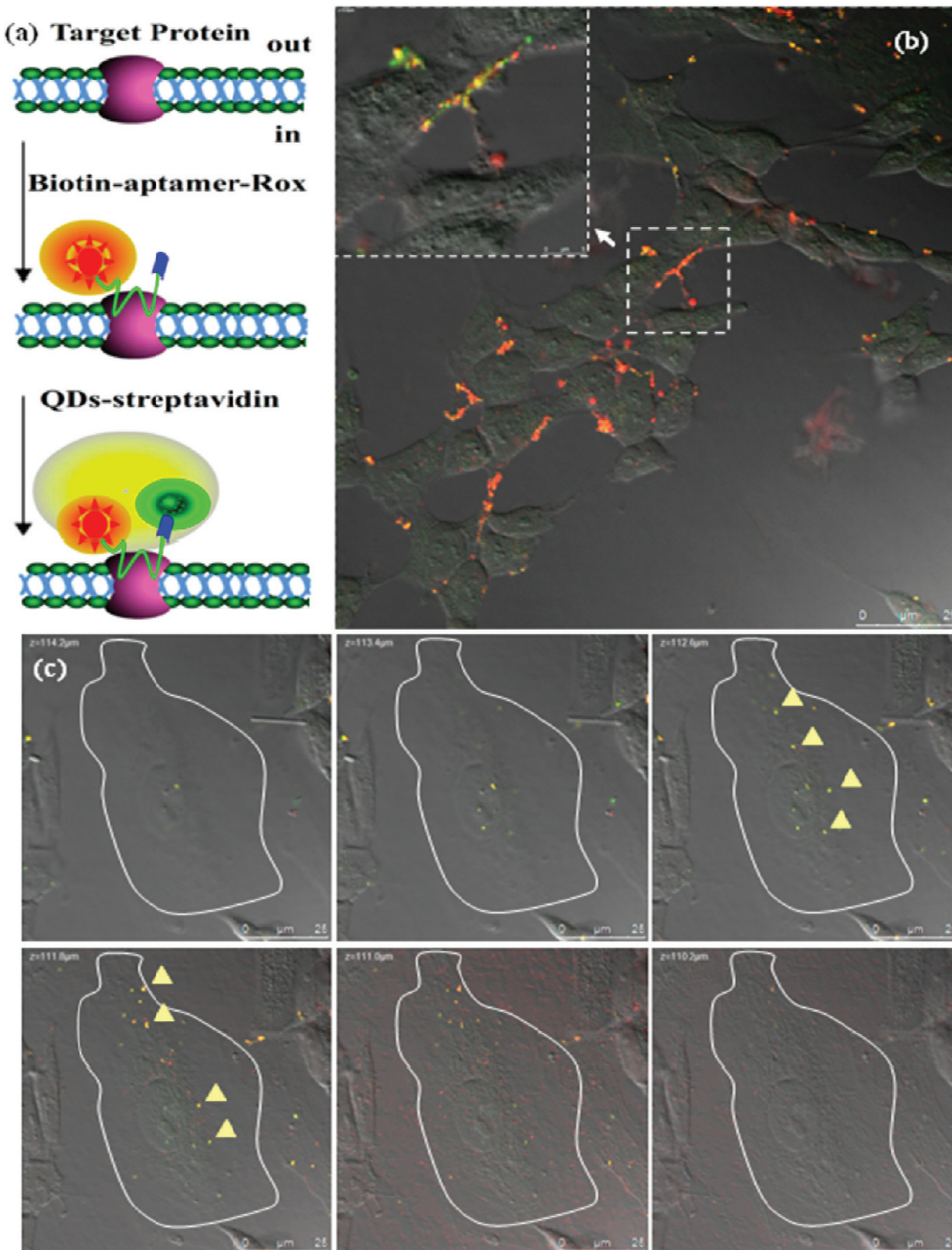


**Figure 2.** Double-color labeling of cellular proteins. (a) Schematic illustration of our strategy for double-color labeling of a protein. In the first step, the cell surface target protein was labeled with Bio-Apt2-ROX, showing a red fluorescent signal. Then the biotinylated protein was recognized by SA-QDs545 to achieve two-color labeling. Owing to the overlap of ROX (red) and QDs545 (green), QD545 target proteins show yellow fluorescence. (b) Representative images of intercellular PrP<sup>C</sup> in cells using the double-color labeling technique. The left upper image represents the local large view in the central panel, showing many yellow particles on the cell membrane. (c) *z* axis scanning of internalized QDs45-PrP<sup>C</sup>-ROX conjugates in SK-N-SH cells revealed by confocal microscopy. Multiple yellow particles (arrowheads) are observed inside the cells at different focal plane distances. The cell boundary is defined with a white line.

identified the double functions of Bio-Apt1 during the labeling processes and also excluded the false signals resulting from unspecific binding of SA-QDs605 in living cells.

**Generality.** To test the generality of our strategy, we replaced the signal reporter of SA-QDs605 with streptavidin-conjugated silver nanoparticles (SA-AgNPs) or streptavidin-conjugated gold nanoparticles (SA-AuNPs). The features of both SA-AgNPs and SA-AuNPs were carefully identified and

characterized before they were used (Figure S3 in the Supporting Information). After incubation with cells as described, dark-field light scattering imaging clearly illustrated that a large number of SA-AgNPs exhibiting blue and green dots (Figure 1b) and SA-AuNPs showing yellow dots (Figure 1c) were bound to HeLa cells in the presence of Bio-Apt1, but the signal was abolished by omitting the Bio-Apt1 (Figures 1e,f). The multicolor exhibited from SA-AgNPs and SA-

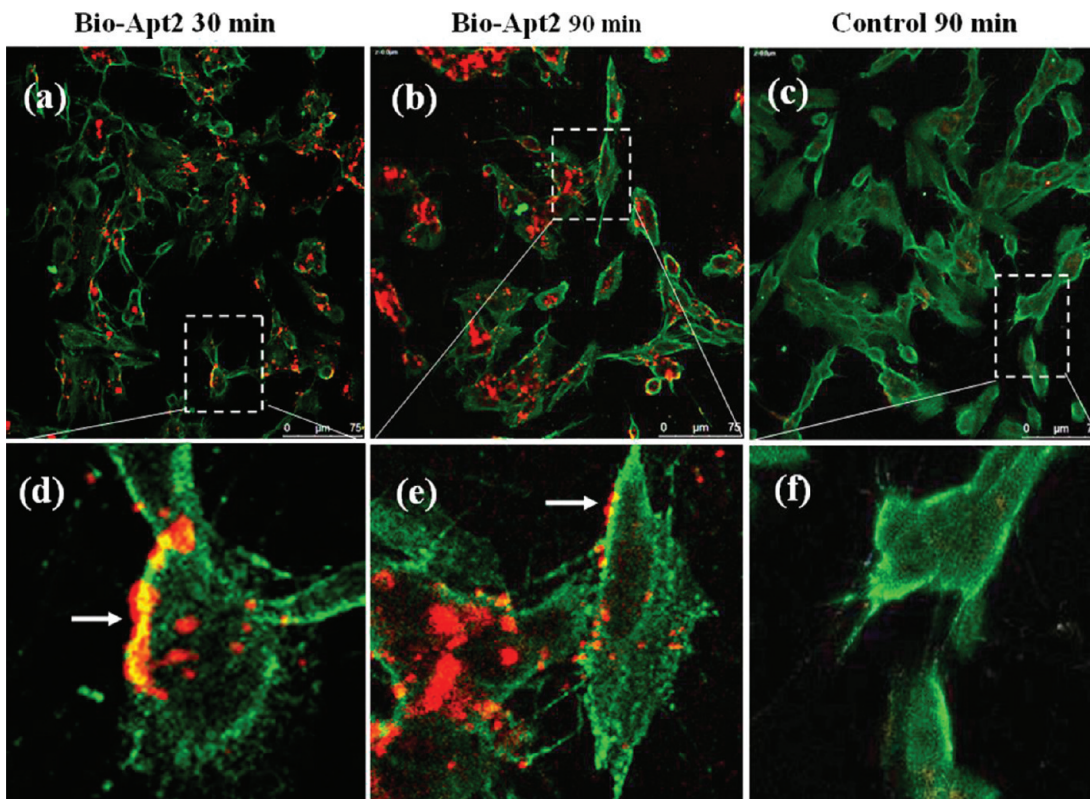


**Figure 3.** Laser confocal scanning microscopy images of  $\text{PrP}^{\text{C}}$ -Apt-QD605 complexes in SK-N-SH cells. (a, d)  $\text{PrP}^{\text{C}}$  labeled with QDs displayed good overlap (yellow color) with the plasma membrane (green color) after 30 min of incubation in the presence of Bio-Apt2. (b, e) After 90 min of incubation, while most of the  $\text{PrP}^{\text{C}}$ -Apt-QD605 conjugates (red color) were transported into the cytoplasm, a small fraction were still visible on the cell membrane. (c, f) No obvious QD605 signal was detected in the control group. DIO and QDs605 are shown in green color and red color, respectively. The lower images are the local large views of the pane in the respective upper images. Arrows indicate the colocalization of QD-labeled  $\text{PrP}^{\text{C}}$  with the plasma membrane.

AuNPs under dark-field microscopy is closely related to their photophysical properties<sup>11,25</sup> since light-scattering properties of metal nanoparticles are dependent on the composition, size, and shape of the nanoparticles as well as their surrounding medium according to the Rayleigh and Mie theory.<sup>27</sup> What is important, these results identified the generality of our strategy and also illustrated its potential for protein labeling and imaging in living cells by using various kinds of nanoparticles.

Nucleolin is able to be expressed at a high level on the surface of HeLa cells, so it is robust to experimental manipulation. However,  $\text{PrP}^{\text{C}}$ , a cell surface glycosylphosphatidylinositol (GPI)-anchored protein which is constitutively internalized into the cytoplasm of human bone marrow neuroblastoma (SK-N-SH cells),<sup>28</sup> poses a more challenging test of our labeling strategy and allows us to determine whether we can use the aptamer-mediated strategy as a powerful tool for analyzing the dynamics of intercellular protein trafficking. Herein, another biotin-modified 17-mer DNA aptamer (Bio-Apt2) that has been identified to specifically recognize residues 23–90 of  $\text{PrP}^{\text{C}}$  was chosen for further testing.<sup>22</sup>

Similarly to the method preliminarily mentioned, after incubation of host cells with Bio-Apt2 and SA-QDs605, a red fluorescent signal was clearly detected, suggesting the form of  $\text{PrP}^{\text{C}}$ -Apt2-QD605 conjugates in SK-N-SH cells, whereas replacing Bio-Apt2 with Bio-PolyT<sub>17</sub> completely abolished labeling (Figure S4 in the Supporting Information). This result demonstrated that cell surface  $\text{PrP}^{\text{C}}$  was successfully labeled by

QDs605 and once again confirmed the generality of our proposed labeling method.

**Double-Color Labeling in Living Cells.** Double-color labeling of proteins in living cells allows more reliable information to be offered by eliminating the influence of false signals from illuminators which were internalized by non-specific endocytosis of cells, but poses an enormous challenge because of the difficulties in targeting two illuminators in one protein synchronously.<sup>12</sup> To challenge our strategy, we further develop a novel double-color label experiment using a dual-functional aptamer whose 5'-terminus is modified with biotin and 3'-terminus is tagged by fluorescent 6-carboxy-X-rhodamine (Bio-Apt2-ROX). As illustrated in Figure 2a, our double-color labeling process is quite simple and practical, and the only difference from single-color labeling is replacement of Bio-Apt with a dual-modified aptamer, namely, Bio-Apt2-ROX conjugates.

Similarly to the single-color labeling procedure, host cells for double-color labeling were first incubated with Bio-Apt2-ROX for 15 min, and then SA-QDs545 were added. As Figure 2b shows, multiple-color dots, including green, red, and yellow, were readily detected in the cell body after incubation for 30 min. The local enlarged image on the upper left clearly shows the yellow overlapping of the plasma membrane and neuraxon, demonstrating the formation of QDs545- $\text{PrP}^{\text{C}}$ -ROX complexes since the yellow dots are only presented when the green SA-QDs545 and red ROX bind together.

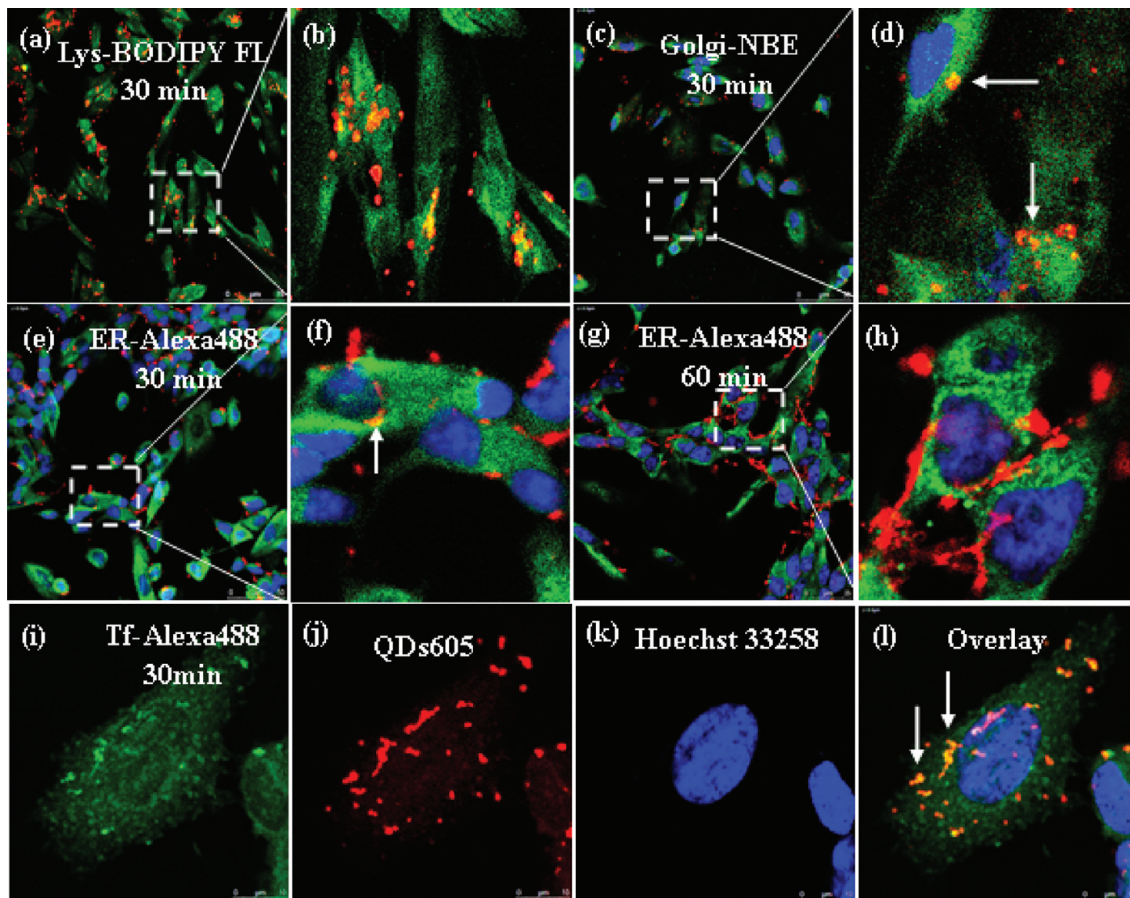


**Figure 4.** Immunocolocalization assays identify intracellular distribution of QD-labeled  $\text{PrP}^{\text{C}}$  after endocytosis in SK-N-SH cells. After 30 min of incubation, QD-labeled  $\text{PrP}^{\text{C}}$  was colocalized with lysosomes (green) (a, b) and the Golgi apparatus (green) (c, d). A small number of  $\text{PrP}^{\text{C}}\text{-Apt}\text{-QD}$  complexes were colocalized with endoplasmatic reticulum (green) after binding and internalization for 30 min (e, f), but the correlation was lost after a longer (60 min) of incubation (g, h). (i–l) Intracellular trafficking of Tf-Alexa488 conjugates overlapped with that of  $\text{PrP}^{\text{C}}$  labeled with QDs605. The right images are the local large views of the pane in the respective left images. Nucleolus dyeing with Hoechst 33258 is shown in blue color.

To further confirm that both Bio-Apt2-ROX conjugates and SA-QDs545 remain associated with  $\text{PrP}^{\text{C}}$  after internalization at progressive time points during endocytosis, we performed vertical section scanning along the  $z$  axis. A typical  $z$  section is reported in Figure 2c. Multiple yellow particles were observed inside the cells at different focal plane distances, illustrating that QD545- $\text{PrP}^{\text{C}}$ -ROX complexes are kept assembled and have been transported into the cytoplasm through a  $\text{PrP}^{\text{C}}$ -dependent endocytic pathway in SK-N-SH cells. These results demonstrated that our aptamer-mediated double-color labeling method can be successfully used for specifically labeling membrane proteins and showed great promise for tracking the endocytic pathway of membrane proteins.

Although multiplex color imaging of a single tumor cell was achieved by Kim's group recently using quantum-dot-conjugated aptamers,<sup>12</sup> our proposal of a double-color labeling method is still unique and attractive. Using a single aptamer, our approach can target two signal reporters in one protein synchronously; as a result, two binding sides in one target protein are not necessary for double-signal labeling, which may open the door for a new aptamer-mediated double-color labeling method. Moreover, our approach also allows two types of signals to be detected simultaneously if different reporters, i.e., fluorescent illuminators or nuclear magnetic resonance

(NMR) nanoprobes, are targeted to the proteins of interest synchronously.

**Subcellular Distribution and Location.** Having established the specificity of Bio-Apt2-directed SA-QD labeling for cell surface  $\text{PrP}^{\text{C}}$ , we then investigated the traffic of  $\text{PrP}^{\text{C}}\text{-Apt}\text{-QD}605$  conjugates in the cytoplasm of cells. After 30 min of incubation, as parts a and d of Figure 3 show, the QD605 conjugates (red dots) displayed good overlap (yellow) with the plasma membrane marker of DIO (green), indicating the target proteins were located in the cell membrane. After their endocytosis was monitored for 90 min, a majority ( $\sim 70\text{--}80\%$ ) of the endocytosed  $\text{PrP}^{\text{C}}\text{-Apt}\text{-QD}605$  conjugates were transported into the cytoplasm, exhibiting a bright red signal; only a small fraction were still visible on the cell membrane (Figure 3b,e). Notably, with long-time incubation, more and more  $\text{PrP}^{\text{C}}\text{-Apt}\text{-QD}605$  conjugates seem likely to be transported into the cytoplasm through a  $\text{PrP}^{\text{C}}$ -dependent endocytic pathway. In contrast, the QD605 signal was observed neither on the membrane nor in the cytoplasm in the control group without Bio-Apt2 treatment (Figure 3c,f).

We further elucidated the entry steps of  $\text{PrP}^{\text{C}}$ -mediated uptake and the subsequent endocytic pathway by establishing the degree of colocalization of the QD605 signals with cellular compartment markers. After 30 min of incubation, a significant number of QDs605 (red) colocalized with lysosome compart-

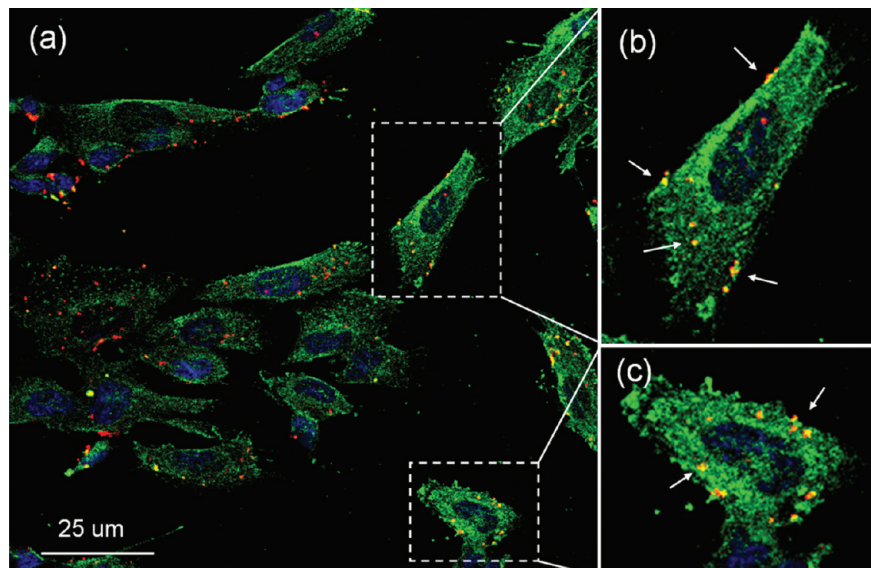


**Figure 5.** Immunofluorescence assays identify clathrin-dependent endocytosis of  $\text{PrP}^{\text{C}}$ -Apt-QD605 complexes. (a) A large number of  $\text{PrP}^{\text{C}}$ -Apt-QD complexes (red) colocalized with intracellular clathrin (green) showing many yellow dots (white arrow) in SK-N-SH cells, and the right two images (b, c) are the local large views of the pane in the respective left image. Cells were incubated with rabbit anticlathrin heavy chain antibody at 1/500 dilution (in 1% BSA/PBS) for 1 h at 22 °C. An Alexa Fluor 488-conjugated goat polyclonal rabbit IgG (H+L) was used as a secondary antibody at 1/400 dilution. Nucleolus dyeing with Hoechst 33258 is shown in blue color.

ment markers (green), as shown by the yellow dots in the cell body, indicating that a fraction of  $\text{PrP}^{\text{C}}$ -Apt-QD605 complexes were transported into lysosomes via the endocytosis pathway (Figure 4a,b). On the contrary, only a few  $\text{PrP}^{\text{C}}$ -QD605 complexes have been visualized colocalizing with Golgi markers (green) of 6-((*N*-(7-nitrobenz-2-oxa-1,3-diazol-4-yl)-amino)hexanoyl)sphingosine (NBD) after binding and internalization for 30 min (Figure 4c,d). Similarly, a small number of QDs605 colocalized with endoplasmatic reticulum (ER) markers (green) after binding and internalization for 30 min (Figure 4e,f), but the correlation was lost after comparatively long-time incubation (60 min) even if more QDs605 were transported into the cytoplasm (Figure 4g,h). These results are consistent with previous reports that, after being endocytosed, only a fraction of  $\text{PrP}^{\text{C}}$  was routed from endosomes and into the Golgi apparatus and further retrogradely transported to the endoplasmatic reticulum from where they were translocated into the cytosol, exerting their neural signal transport effect.<sup>29</sup>

It is well-known that transferrin (Tf) internalized through clathrin-dependent/receptor-mediated endocytosis, which is partially similar to the internalization pathway of  $\text{PrP}^{\text{C}}$ .<sup>30</sup> In this context, transferrin-Alexa488 conjugates (Tf-Alexa488) were used as a control to elucidate whether endocytosis or intracellular trafficking of Tf could overlap with that of  $\text{PrP}^{\text{C}}$  labeled with QDs605. As shown in Figures 4i–l, fluorescence signals of QDs605 and Tf-Alexa488 were colocalized in the cytoplasm of SK-N-SH cells, confirming that the internalization pathways of Tf-Alexa488 and QD605-labeled  $\text{PrP}^{\text{C}}$  partially overlap. Previous work with either immunofluorescence or immunocolloid gold label methods has demonstrated that  $\text{PrP}^{\text{C}}$  and TfR were colocalized in early endosomes.<sup>31</sup> Clathrin is a protein which assembles into a polyhedral network on the cell membrane, forming a coated pit which is essential to  $\text{PrP}^{\text{C}}$  endocytosis.<sup>29</sup> To investigate the internalized pathway of  $\text{PrP}^{\text{C}}$ -QD conjugates, we used immunofluorescence colocalized assays to identify whether clathrin-dependent endocytosis is a necessary pathway. Figure 5 shows that a large number of

$\text{PrP}^{\text{C}}$ -Apt-QD complexes (red) colocalized with intracellular clathrin (green), exhibiting many yellow dots in SK-N-SH cells, demonstrating  $\text{PrP}^{\text{C}}$ -Apt-QD complexes most likely internalized into the cytoplasm through a classical clathrin-dependent/receptor-mediated pathway.

The intracellular routes and fate of nanoparticles are dependent on the physiology of the host cells studied as well as the physiochemical properties of the nanoparticle–biomolecule complexes. Our studies show several lines of evidence that are consistent with the idea that  $\text{PrP}^{\text{C}}$ -QD conjugates follow a process that is similar to that of  $\text{PrP}^{\text{C}}$  during endocytosis: (1) the fluorescent colocalization assay shows that a majority of  $\text{PrP}^{\text{C}}$ -Apt-QD conjugates can cross the membrane to be transported into the cytosol, but QDs almost cannot; (2) a significant number of  $\text{PrP}^{\text{C}}$ -Apt-QD complexes colocalize with lysosome at 30 min, but only a few  $\text{PrP}^{\text{C}}$ -Apt-QD complexes colocalize with the Golgi complex at the same time point; (3) a small number of  $\text{PrP}^{\text{C}}$ -QD605 complexes colocalize with the endoplasmatic reticulum at time periods up to 30 min, but correlation is lost at 60 min; (4)  $\text{PrP}^{\text{C}}$ -Apt-QD complexes colocalize with transferrin receptors and clathrin. Although further studies will be needed to trace the exact vesicular pathway that  $\text{PrP}^{\text{C}}$ -Apt-QD605 complexes pass through after internalization, these initial lines of evidence indicate that  $\text{PrP}^{\text{C}}$ -Apt-QD605 complexes internalized into the cytoplasm through a clathrin-dependent/receptor-mediated pathway, namely,  $\text{PrP}^{\text{C}}$  tagged with QDs underwent a normal internalization pathway of  $\text{PrP}^{\text{C}}$ . These results suggest that our labeling method is unlikely to perturb the target proteins' internalization and transportation and can be used for mapping specific protein trafficking pathways in cells and correlating this to discrete protein dynamics.

**Single-Particle Tracking and Dynamic Analysis.** Extremely bright and photostable QDs have been widely used in studying the molecular scale dynamics in live cells,<sup>32,33</sup> for example, studies of the endocytic dynamics of nerve growth factor receptors (NGFRs).<sup>1</sup> However, very limited applications

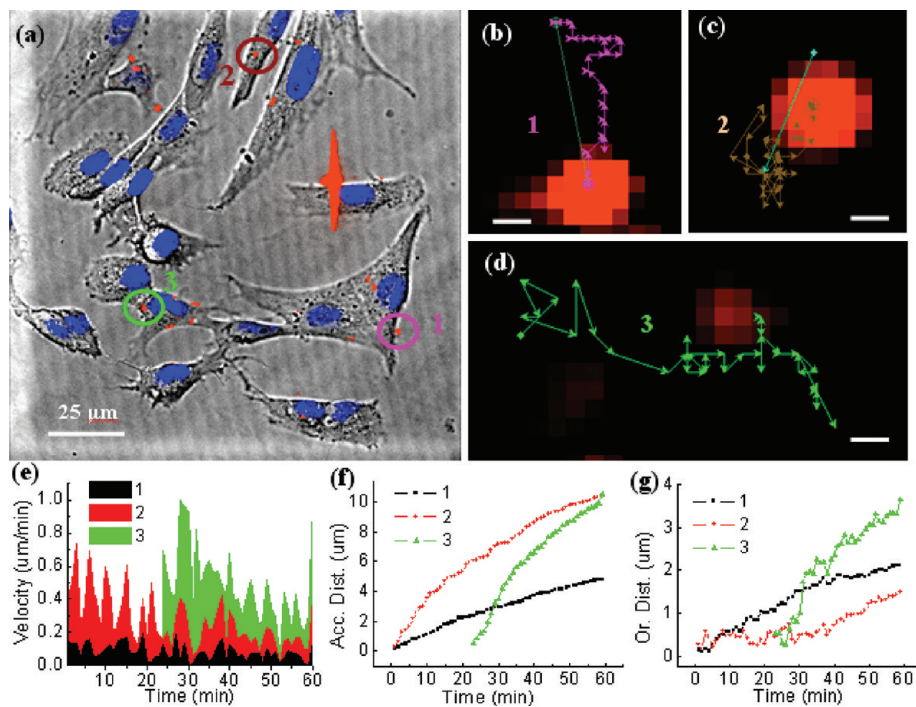


**Figure 6.** Real-time imaging and dynamic analysis of  $\text{PrP}^{\text{C}}$ -Apt-QD605 complexes in living cells. (a) Representative images of cells after treatment with Bio-Apt2 and SA-QDs for 30 min. (b-d) Representative trajectories of three types of movements. The bar is 1  $\mu\text{m}$ . (e-g) Comparison and analysis of the dynamic characteristics, including velocity, accumulated distance (Acc. Dist.), and distance from the original starting point (Or. Dist.) of three types of transport of  $\text{PrP}^{\text{C}}$ -Apt-QD605 complexes in living cells.

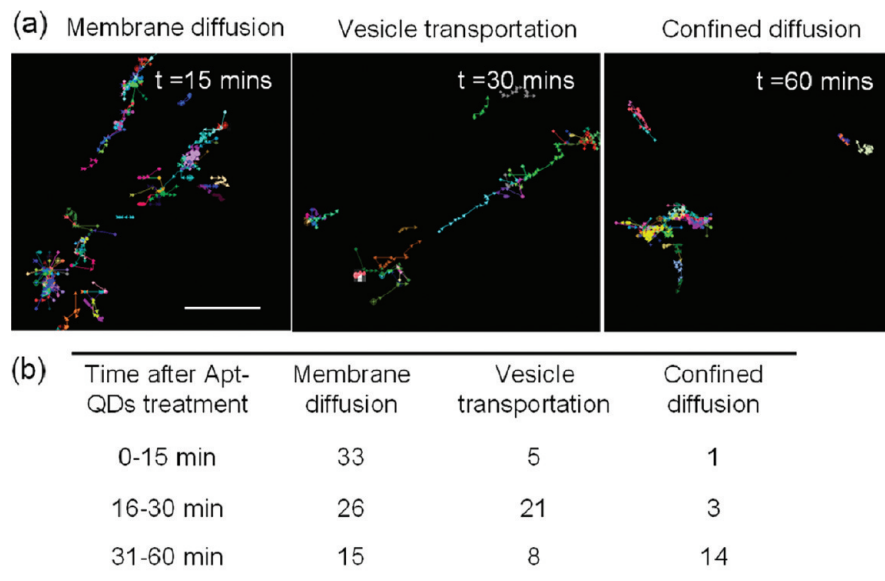


**Figure 7.**  $\text{PrP}^{\text{C}}$ -Apt-QD complexes exhibit three distinct movements at progressive phases of endocytic trafficking. (a) Trajectories of  $\text{PrP}^{\text{C}}$ -Apt-QD complexes at progressive time points show synchronized phases of movement: membrane diffusion, vesicle transportation, and confined diffusion. The bar is 1  $\mu\text{m}$ . (b) Table showing the number of trajectories categorized by the type of movement at each time interval. A total of 126  $\text{PrP}^{\text{C}}$ -Apt-QD trajectories of 300 s duration were examined from three independent experiments.

were found in the dynamic tracking of disease-related proteins using aptamer-QD conjugates, and rare information about the real-time dynamic intracellular transport of  $\text{PrP}^{\text{C}}$  was available,<sup>34</sup> although various hypotheses for the  $\text{PrP}^{\text{C}}$  endocytic mechanisms were offered.<sup>29</sup> Herein, to test the versatility of our approach, we made use of the photophysical properties of QDs to track the movements and to analyze the dynamics of Apt2-QD-tagged  $\text{PrP}^{\text{C}}$  in SK-N-SH cells. The time-lapse images

illustrated the kinetics of accumulation of  $\text{PrP}^{\text{C}}$ -Apt-QD605 complexes at the cell surface and in the cytoplasm (as shown in Figure S5, Supporting Information). After 30 min of incubation, most of the detectable  $\text{PrP}^{\text{C}}$ -Apt-QD605 complexes were transported into the intracellular compartments, while only a few complexes stuck to the surface of the neuroblastoma cells (Figure 6a). To monitor and analyze the kinetics of  $\text{PrP}^{\text{C}}$ -Apt-QD605 complexes inside the cells, we

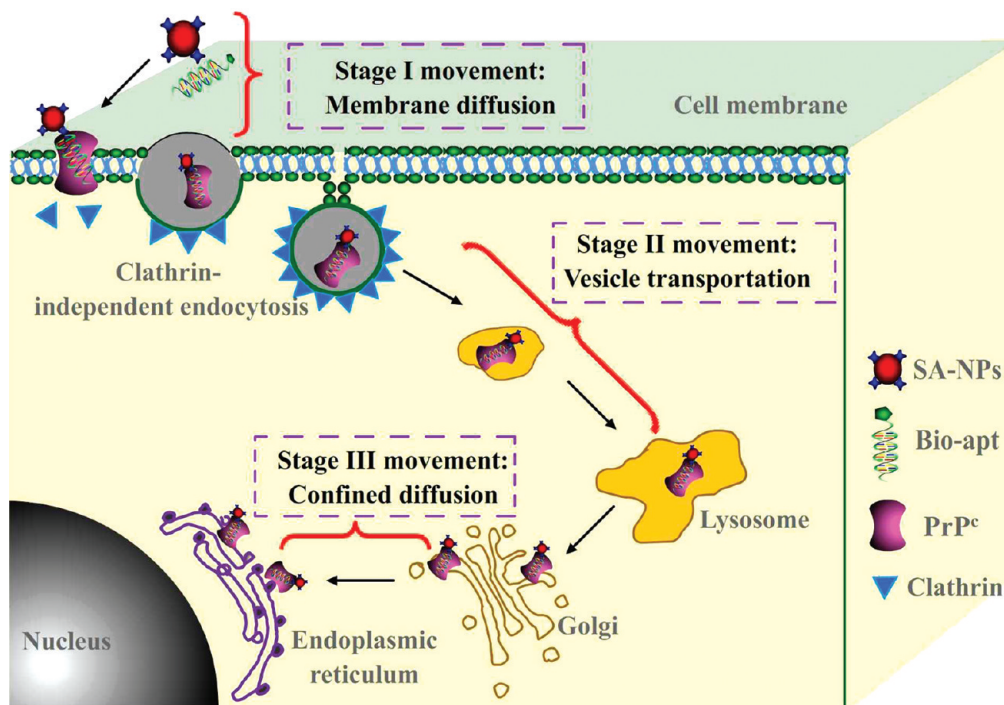


**Figure 8.** Model of the dynamic characteristics of the PrP<sup>c</sup>-Apt-QD complex toward its pathway of clathrin-independent endocytosis. Three phases of movement that occurred at distinct times of endocytosis are included, namely, membrane diffusion, vesicle transportation, and confined diffusion. After incubation with Bio-Apt and SA-QDs, a PrP<sup>c</sup>-Apt-QD complex is formed and then internalized by clathrin-independent endocytosis (stage I movement). Next, PrP<sup>c</sup>-Apt-QD complexes undergo a long-distance transport from the clathrin-coated pit to the lysosome via vesicle transportation (stage II movement). Later, a certain number of PrP<sup>c</sup>-Apt-QD complexes attach onto or fall into the cellular organelles, such as the Golgi apparatus or endoplasmic reticulum, exhibiting confined diffusion (stage III movement).

randomly tracked a large set of individual PrP<sup>c</sup>-Apt-QD605 complexes ( $n = 75$ ) and then categorized the motion of these complexes into three representative types according to their dynamic characteristics.

The first type of particle ( $n = 15$ ) moved slowly on the cell surface with a very low velocity of about  $0.1 \mu\text{m}/\text{min}$  and a small displacement of  $4 \mu\text{m}$  (Figure 6b,e,f). This was most evident at  $t = 1\text{--}15 \text{ min}$ , when a majority of PrP<sup>c</sup>-Apt-QD conjugates had moved from the membrane surface into the cytosol, and the motion of PrP<sup>c</sup>-Apt-QD conjugates remaining on the membrane could be followed at durations of  $15\text{--}30 \text{ min}$ . The second type of particle ( $n = 39$ ) underwent only slight and nondirectional movements with a medium velocity from  $0.2$  to  $0.6 \mu\text{m}/\text{min}$ , yet showing a long accumulated distance (Acc. Dist.) of about  $10 \mu\text{m}$  that was interrupted by many stops (Figure 6c,e,f). It is worth noting that there is an obvious difference between Acc. Dist. and the distance from the original starting point (Or. Dist.) of the second representative transport of the PrP<sup>c</sup>-Apt-QD605 complex (see the red curve in Figure 6e-g). With a medium velocity and the longest Acc. Dist., the second representative transport, however, moved only the shortest Or. Dist. of  $2 \mu\text{m}$ , even shorter than that of the first type of transport.

The nature of these movements suggests that the PrP<sup>c</sup>-Apt-QD605 complexes undergo restricted diffusion, which is defined as a nondirectional movement that is reversible, strays away, and then returns to the original point.<sup>1</sup> These nondirectional movements likely represent the attachment of PrP<sup>c</sup>-Apt-QD605 complexes to the cytosolic structures, such as the ER or Golgi apparatus, which are known to possess immovable properties. In contrast, the third type of particle ( $n = 21$ ) transported with the same direction showed a rather

continuous movement at a constant speed of  $0.6 \mu\text{m}/\text{min}$  with little pause, and thus, a long-range distance from Or. Dist. of  $4 \mu\text{m}$  can be reported (Figure 6d-f). The presence of sustained linear trajectories allows us to assume that the PrP<sup>c</sup>-Apt-QD605 complex cargo is likely transported a certain distance before it gets away from the lysosome.

To further determine if these general classes of movement were associated with distinct phases of endocytosis, a total of 126 PrP<sup>c</sup>-Apt-QD trajectories were examined from three independent experiments. As Figure 7a shows, trajectories of PrP<sup>c</sup>-Apt-QD complexes at progressive time points show synchronized phases of movement: membrane diffusion, vesicle transportation, and confined diffusion. The table in Figure 7b shows a cumulative summary that indicates that PrP<sup>c</sup>-Apt-QD605 conjugates exhibit movements synchronized with distinct endocytic phases.

Combining previous results<sup>34</sup> and findings from this work, we proposed a model of the dynamics of PrP<sup>c</sup>-Apt-QD conjugates at progressive phases of endocytic trafficking (Figure 8). Three phases of movement were suggested that occurred at distinct times during endocytosis, including membrane diffusion, vesicle transportation, and confined diffusion. As for membrane diffusion, which occurs immediately following Bio-Apt and SA-QD treatment, the PrP<sup>c</sup>-Apt-QD conjugates exhibited diffusive movement ( $t = 1\text{--}15 \text{ min}$ ). This phase may also involve a protein transmembrane movement in which the PrP<sup>c</sup>-Apt-QD conjugate was internalized into the cytoplasm through a pathway of clathrin-independent endocytosis. As for vesicle transportation, which occurs after internalization, many PrP<sup>c</sup>-Apt-QD complexes exhibited cytoplasmic vesicle trafficking ( $t = 15\text{--}30 \text{ min}$ ). This phase was characterized by linear, directed movements, a long-range distance, and a rapid

transport speed. As for confined diffusion, which occurs after vesicle transportation, PrP<sup>C</sup>-Apt-QD complexes could attach to the cytosolic structures, i.e., the ER or Golgi apparatus. As a consequence, they exhibited diffusive-based dynamics of confined movement, and the trajectories were confined to movement within spherical regions ( $t = 30\text{--}60\text{ min}$ ).

This model shows a cumulative summary that indicates that three general classes of movement of PrP<sup>C</sup>-Apt-QD complexes were associated with distinct phases of PrP<sup>C</sup> endocytosis. As PrP<sup>C</sup> is a critical protein exploiting the cell's constitutive endocytic pathway for pathogen infection, the model derived here (Figure 8) should have general implications for the studies of dynamic processes of protein endocytosis. Most importantly, all these data derived from both dynamic analysis and trajectory mapping identified the feasibility of our aptamer-directed nanoparticle-based strategy and indicated its great potential for cellular protein tracking and dynamic analysis in real time.

## CONCLUSION

In this work, we proposed a novel and general strategy by employing aptamers not only as the identifier for specific protein recognition but also as the linker for targeting SA-NPs to the proteins of interest to specifically label membrane proteins and track their endocytic pathway. The utility of this novel strategy was well demonstrated in various types of experiments, including single-color or two-color fluorescence labeling, investigation of the subcellular distribution of proteins, and dynamic tracking of single protein in living cells, and then a model of the dynamics of PrP<sup>C</sup>-Apt-QD conjugates at progressive phases of endocytic trafficking was proposed, which includes membrane diffusion, vesicle transportation, and confined diffusion. Compared with traditional methods, this novel strategy is simple in procedure, avoiding any complicated probe modification and purification. Moreover, this strategy is general since various aptamers for specific disease-related protein targeting have been selected and identified.

Although we used this approach for visualization of nucleolin and prion protein, the strategy is versatile by selecting not only different sequences of aptamers for other disease-related proteins such as platelet-derived growth factors (PDGF)<sup>35</sup> and angiogenin<sup>7</sup> to investigate the protein of interest but also different types of nanoreporters, such as fluorescent nanoprobes, NMR nanoprobes, and multisignal complex nanoprobes so that it allows multiple signals to be detected simultaneously.<sup>36–38</sup> In addition, because the biotin detection by streptavidin is one of the tightest interactions ( $K_d = 10^{-13}\text{ M}$ ),<sup>39</sup> this method may be highly promising for monitoring the rapid dynamic processes of disease-related proteins in real time. Our present strategy may provide new insight into the use of multifunctional aptamers as a comprehensive tool for targeting nanoparticles to proteins and elucidating the molecular details of intracellular transport of many kinds of disease-related proteins in living cells.

## ASSOCIATED CONTENT

### Supporting Information

Five additional figures as noted in text. This material is available free of charge via the Internet at <http://pubs.acs.org>.

## AUTHOR INFORMATION

### Corresponding Author

\*E-mail: chengzhi@swu.edu.cn. Phone/fax: 86-23-68254659.

### Notes

The authors declare no competing financial interest.

## ACKNOWLEDGMENTS

This work has been financially supported by the Ministry of Science and Technology of the People's Republic of China (Grant 2011CB933600) and the National Natural Science Foundation of China (NSFC; Grant 21035005).

## REFERENCES

- (1) Rajan, S. S.; Liu, H. Y.; Vu, T. Q. *ACS Nano* **2008**, *2*, 1153–1166.
- (2) Ruan, G.; Agrawal, A.; Marcus, A. I.; Nie, S. *J. Am. Chem. Soc.* **2007**, *129*, 14759–14766.
- (3) Resch-Genger, U.; Grabolle, M.; Cavaliere-Jaricot, S.; Nitschke, R.; Nann, T. *Nat. Methods* **2008**, *5*, 763–775.
- (4) Howarth, M.; Takao, K.; Hayashi, Y.; Ting, A. Y. *Proc. Natl. Acad. Sci. U.S.A.* **2005**, *102*, 7583–7588.
- (5) Chen, I.; Ting, A. Y. *Curr. Opin. Biotechnol.* **2005**, *16*, 35–40.
- (6) Kong, R.-M.; Zhang, X.-B.; Chen, Z.; Tan, W. *Small* **2011**, *7*, 2428–2436.
- (7) Li, W.; Yang, X.; Wang, K.; Tan, W.; He, Y.; Guo, Q.; Tang, H.; Liu, J. *Anal. Chem.* **2008**, *80*, 5002–5008.
- (8) López-Colón, D.; Jiménez, E.; You, M.; Gulbakan, B.; Tan, W. *Wiley Interdiscip. Rev. Nanomed. Nanobiotechnol.* **2011**, *3*, 328–340.
- (9) Xiao, S. J.; Hu, P. P.; Wu, X. D.; Zou, Y. L.; Chen, L. Q.; Peng, L.; Ling, J.; Zhen, S. J.; Zhan, L.; Li, Y. F.; Huang, C. Z. *Anal. Chem.* **2010**, *82*, 9736–9742.
- (10) Cui, Z.-Q.; Ren, Q.; Wei, H.-P.; Chen, Z.; Deng, J.-Y.; Zhang, Z.-P.; Zhang, X.-E. *Nanoscale* **2011**, *3*, 2454–2457.
- (11) Chen, L. Q.; Xiao, S. J.; Peng, L.; Wu, T.; Ling, J.; Li, Y. F.; Huang, C. Z. *J. Phys. Chem. B* **2010**, *114*, 3655–3659.
- (12) Kang, W. J.; Chae, J. R.; Cho, Y. L.; Lee, J. D.; Kim, S. *Small* **2009**, *5*, 2519–2522.
- (13) Bagalkot, V.; Zhang, L.; Levy-Nissenbaum, E.; Jon, S.; Kantoff, P. W.; Langer, R.; Farokhzad, O. C. *Nano Lett.* **2007**, *7*, 3065–3070.
- (14) Medley, C. D.; Bamrungsap, S.; Tan, W.; Smith, J. E. *Anal. Chem.* **2011**, *83*, 727–734.
- (15) Farokhzad, O. C.; Cheng, J.; Teply, B. A.; Sherifi, I.; Jon, S.; Kantoff, P. W.; Richie, J. P.; Langer, R. *Proc. Natl. Acad. Sci. U.S.A.* **2006**, *103*, 6315–6320.
- (16) Sweeney, S. F.; Woehrle, G. H.; Hutchison, J. E. *J. Am. Chem. Soc.* **2006**, *128*, 3190–3197.
- (17) Chen, I.; Howarth, M.; Lin, W.; Ting, A. Y. *Nat. Methods* **2005**, *2*, 99–104.
- (18) Bonasio, R.; Carman, C. V.; Kim, E.; Sage, P. T.; Love, K. R.; Mempel, T. R.; Springer, T. A.; von Andrian, U. H. *Proc. Natl. Acad. Sci. U.S.A.* **2007**, *104*, 14753–14758.
- (19) Sunbul, M.; Yen, M.; Zou, Y.; Yin, J. *Chem. Commun.* **2008**, *45*, 5927–5929.
- (20) Joo, K.-I.; Lei, Y.; Lee, C.-L.; Lo, J.; Xie, J.; Hamm-Alvarez, S. F.; Wang, P. *ACS Nano* **2008**, *2*, 1553–1562.
- (21) Girvan, A. C.; Teng, Y.; Casson, L. K.; Thomas, S. D.; Jülicher, S.; Ball, M. W.; Klein, J. B.; Pierce, W. M.; B., S. S. Jr.; Bates, P. J. *Mol. Cancer Ther.* **2006**, *5*, 1790–1799.
- (22) Takemura, K.; Wang, P.; Vorberg, I.; Surewicz, W.; Priola, S. A.; Kanthasamy, A.; Pottathil, R.; Chen, S. G.; Sreevatsan, S. *Exp. Biol. Med.* **2006**, *231*, 204–214.
- (23) Lee, P. C.; Meisel, D. *J. Phys. Chem.* **1982**, *86*, 3391–3395.
- (24) David D. Evanoff, J.; Chumanov, G. *J. Phys. Chem. B* **2004**, *108*, 13957–13962.
- (25) Ling, J.; Li, Y. F.; Huang, C. Z. *Anal. Chem.* **2009**, *81*, 1707–1714.
- (26) Christian, S.; Pilch, J.; Akerman, M. E.; Porkka, K.; Laakkonen, P.; Ruoslahti, E. *J. Cell Biol.* **2003**, *168*, 871–878.

- (27) Yguerabide, J.; Yguerabide, E. E. *Anal. Biochem.* **1998**, *262*, 137–156.
- (28) Stahl, N.; Borchelt, D. R.; Hsiao, K.; Prusiner, S. B. *Cell* **1987**, *51*, 229–240.
- (29) Linden, R.; Martins, V. R.; Prado, M. A. M.; Cammarota, M.; Izquierdo, I.; Brentani, R. R. *Physiol. Rev.* **2008**, *88*, 673–728.
- (30) Morris, R. J.; Parkyn, C. J.; Jen, A. *FEBS Lett.* **2006**, *580*, 5565–5571.
- (31) Sunyach, C.; Jen, A.; Deng, J.; T.Fitzgerald, K.; Frobert, Y.; Grassi, J.; W.McCaffrey, M.; Morris, R. *EMBO J.* **2003**, *22*, 3591–3601.
- (32) Qi, L.; Gao, X. *ACS Nano* **2008**, *2*, 1403–1410.
- (33) Cambi, A.; Lidke, D. S.; Arndt-Jovin, D. J.; Figdor, C. G.; Jovin, T. M. *Nano Lett.* **2007**, *7*, 970–977.
- (34) Tsuji, T.; Kawai-Noma, S.; Pack, C.-G.; Terajima, H.; Yajima, J.; Nishizaka, T.; Kinjo, M.; Taguchi, H. *Biochem. Biophys. Res. Commun.* **2011**, *405*, 638–643.
- (35) Huang, C.-C.; Huang, Y.-F.; Cao, Z.; Tan, W.; Chang, H.-T. *Anal. Chem.* **2005**, *77*, 5735–5741.
- (36) Choi, J.-S.; Park, J. C.; Nah, H.; Woo, S.; Oh, J.; Kim, K. M.; Cheon, G. J.; Chang, Y.; Yoo, J.; Cheon, J. *Angew. Chem., Int. Ed.* **2008**, *47*, 6259–6262.
- (37) Kim, J.; Kim, H. S.; Lee, N.; Kim, T.; Kim, H.; Yu, T.; Song, I. C.; Moon, W. K.; Hyeon, T. *Angew. Chem., Int. Ed.* **2008**, *47*, 8322.
- (38) Park, J.-H.; Maltzahn, G. v.; Ruoslahti, E.; Bhatia, S. N.; Sailor, M. J. *Angew. Chem., Int. Ed.* **2008**, *47*, 7284–7288.
- (39) Piran, U.; Riordan, W. J. *J. Immunol. Methods* **1990**, *133*, 141–143.